Global Analysis of Dynamical Systems
Festschrift dedicated to Floris Takens for his 60th birthday

Edited by
Henk W. Broer, Bernd Krauskopf and Gert Vegter

January 16, 2003

Chapter 1

Global Bifurcations of Periodic Orbits in the Forced van der Pol Equation

John Guckenheimer
Mathematics Department, Cornell University, Ithaca, NY 14853
Kathleen Hoffman
Department of Mathematics and Statistics, University of Maryland, Baltimore County, Baltimore, MD 21250
Warren Weckesser
Mathematics Department, University of Michigan, Ann Arbor MI 48109

1.1 Introduction

The forced van der Pol equation, written in the form

$$
\begin{array}{rcl}
\varepsilon\dot{x} & = & y + x - \frac{x^3}{3} \\
\dot{y} & = & -x + a\sin(2\pi\theta) \\
\dot{\theta} & = & \omega
\end{array}
\tag{1.1}
$$

defines a vector field on $\mathbb{R}^2 \times S^1$. This dynamical system has a long history. It was the system in which Cartwright and Littlewood [2, 10, 11] first noted the existence of chaotic solutions in a dissipative system. They studied the system when $\varepsilon > 0$ is small, the region of relaxation oscillations. Van der Pol and van der Mark [19] observed multistability and hysteresis in experimental studies of an electrical circuit roughly modeled by the van der Pol equation. Following the observations of van der Pol and van der Mark, Cartwright and Littlewood proved that there are parameter values at which the system has two stable periodic orbits of different periods. A theorem of Birkhoff then implies that the basin boundary dividing the basins of attraction of these two periodic orbits cannot be a smooth torus. Eventually, Littlewood produced an intricate analysis proving the existence

of chaotic solutions in the van der Pol equation [11]. Levinson [9] gave a more accessible analysis of a simplified, piecewise linear system that inspired Smale's horseshoe [15]. Levi [8] gave a more comprehensive analysis of a still simpler system. In parameter ranges that are not stiff, periodic orbits of the van der Pol equation have been studied numerically by Mettin et al. [12]. See also Flaherty and Hoppensteadt [4].

Takens [17] took a different approach to proving the existence of chaotic solutions in the van der Pol system, investigating the dynamics associated with codimension two bifurcations in which a periodic orbit has a return map whose linearization has one as an eigenvalue of multiplicity two in a regime where the system is nearly linear. He argued that there should be nearby parameters at which there is a periodic orbit with transversal intersections of its stable and unstable manifolds. If true, the Smale-Birkhoff Theorem implies that there are invariant subsets on which the flow is conjugate to a subshift of finite type. Takens' analysis was based upon the properties of generic vector fields: the splittings between stable and unstable manifolds are "beyond all orders" and cannot be computed using regular perturbation theory. To our knowledge, more sophisticated methods of singular perturbation theory have not been applied to compute these splittings in this example.

Despite the role that this system has played historically, the global dynamics and bifurcations of relaxation oscillations of the force van der Pol equation have not been thoroughly studied, even numerically. When $\varepsilon \leq 10^{-3}$, initial value solvers are unable to follow solutions of the system that lie close to unstable portions of the critical manifold defined by $y = x^3/3 - x$ [6]. Classification of bifurcations from numerical computations is difficult in this regime because the initial value solvers do not resolve the flow near all of the bifurcations. When $\varepsilon = 0$, the character of the equation changes, becoming a differential algebraic equation, similar to the "constrained" systems studied by Takens [18] as models of electrical circuits. The solutions of the singular limit are described by a two dimensional *slow flow* augmented by jumps from fold curves of the critical manifold where existence of solutions to the slow flow equations breaks down. We exploit this structure and investigate the global bifurcations of the differential algebraic equations, including the effects of their jumps.

Previous studies have examined the global geometry of the system in terms of a cross-section to the flow defined by a constant phase of the forcing term. This is a natural thing to do for periodically forced oscillations, replacing the autonomous system as a continuous vector field in its phase plane by a discrete time diffeomorphism. The perspective here is different, however. The nature of the bifurcations of the system and their relationship to the singular limit becomes more transparent when we use a "cross-section" that contains a fold curve of the critical manifold. Our work is based upon the decomposition of trajectories of (1.1) into regular, slow

segments and fast segments that are almost parallel to the x-axis in this system. The singular limit of the return map is then a map of a circle that has discontinuities related to this degenerate decompositions of trajectories. This paper highlights the main features of these return maps and the kinds of bifurcations displayed in the two parameter family of differential algebraic equations.

Asymptotic analysis of the relationship between the slow flow and the van der Pol equation with $\varepsilon > 0$ is subtle and involves "canards," solution segments that follow the unstable sheet of the critical manifold. The chaotic orbits of the van der Pol equation discovered by Cartwright and Littlewood contain canards, and much of their work is devoted to describing the properties of trajectories with canards and developing topological properties of chaotic invariant sets. They did not consider the bifurcations of the stable periodic orbits. We observe here that the bifurcations of these stable periodic orbits persist in the singular limit of the differential algebraic equations, and that they can be located without analysis of canards. The key observation that we make is based upon an examination of where the slow-fast decomposition of trajectories is degenerate. Degenerate decompositions occur when a trajectory jumps from a folded singular point [1] or jumps to a point where the vector field is tangent to the projection of the fold curve along the fast flow. The first type of degeneracy gives rise to canards; the second type of degeneracy is crucial to the existence of periodic orbits of different periods in the van der Pol equation. Tangencies of the vector field with projection of a fold curve onto another sheet of the critical manifold were described briefly by Grasman [5] and Mishchenko et al. [14], but they do not appear to have been described or analyzed previously in the van der Pol equation. This work is descriptive, not rigorous. We unabashedly utilize the results of numerical computations without establishing error estimates or giving proofs.

1.2   The Slow Flow and its Bifurcations

We study the van der Pol system for small values of ε. The limit $\varepsilon = 0$ is a system of *differential algebraic equations* that we shall label the DAE when we want to distinguish it from the slow flow defined by (1.2). The critical manifold of the van der Pol equation is the surface defined by $y = x^3/3 - x$. We shall use coordinates (θ, x) for the critical manifold. We denote the circle defined by $x = c$ by S_c. The projection of the vector field onto the critical manifold is singular on its fold curve, consisting of the circles $S_{\pm 1}$. At most points of the fold curve, trajectories arrive from both sides or they leave from both sides: the existence theorem for ordinary differential equations breaks down for the DAE at these points. However, we know that when $\varepsilon > 0$ is small, trajectories of the van der Pol system are almost

parallel to the x-axis off the critical manifold. Therefore, when trajectories of the DAE arrive at the fold curves $S_{\pm 1}$, we apply a discrete transformation that maps $(\theta, \pm 1)$ to the other point of intersection of a line parallel to the x-axis with the critical manifold, namely $(\theta, \mp 2)$. The exceptions to this rule occur at *folded singularities*, described below. Some trajectories of the van der Pol equation arriving at folded singularities follow the unstable sheet of the critical manifold, jumping at a later time and place. These trajectories are called *canards*. We regard the jumps from fold curves and canards as part of the structure of the DAE. To cope better with the singularity of the DAE, we rescale time to obtain the *slow flow* of the system.

The slow flow of the van der Pol equations is defined by the system

$$
\begin{aligned}
\theta' &= \omega(x^2 - 1) \\
x' &= -x + a\sin(2\pi\theta)
\end{aligned}
\tag{1.2}
$$

These equations are obtained by setting $\varepsilon = 0$ in 1.1, differentiating $y - (x^3/3 - x) = 0$ to yield $\dot{y} = (x^2 - 1)\dot{x}$ and rescaling time by the factor $(x^2 - 1)$. Note that the time rescaling is singular at $x = \pm 1$ and that it reverses the direction of time in $|x| < 1$. This needs to be taken into account when relating the phase portraits of the slow flow to the DAE and to (1.1). We also take into account that there are jumps from fold curves to the circles $S_{\mp 2}$, so that tangencies of the slow flow with these lines will play a special role in our analysis. Singular points of the slow flow occur only when $|a| \geq 1$. These are the folded singularities. They are located on the fold curves at $(\sin^{-1}(\pm 1/a)/(2\pi), \pm 1)$, where $\sin^{-1}$ is regarded as a multi-valued function. They are *not* close to singular points of the full system (there are none), but rather represent points where the direction of motion towards or away from the fold curve changes. Figure 1.1 shows a plot of the critical manifold of the van der Pol equation, the folded singularities, trajectories of the slow flow and a representative trajectory of the van der Pol equation. The role of the folded singularities is apparent in this figure. Trajectories of the van der Pol equation can turn along the critical manifold near the folded singularities without jumping immediately to another sheet.

The limit trajectories of the van der Pol equation with initial points on S_2 follow trajectories of the slow flow to their intersection with S_1. Away from the folded singularities, they then jump to S_{-2}, follow trajectories of the slow flow to S_{-1} where they jump once again to S_2. This cycle defines a return map for the DAE. Trajectories of the DAE that reach a point that is a folded singularity for the slow flow may continue past the singularity, backwards in time along a trajectory of the slow flow in the region $|x| < 1$. These canards may jump to one of the regions with $|x| > 1$ at any point along their trajectories. The jumps of the DAE all occur along lines parallel to the x-axis, so the jump from a point (θ, x) along a canard is to one of the two points (θ, u) where $u^3/3 - u = x^3/3 - x$. The
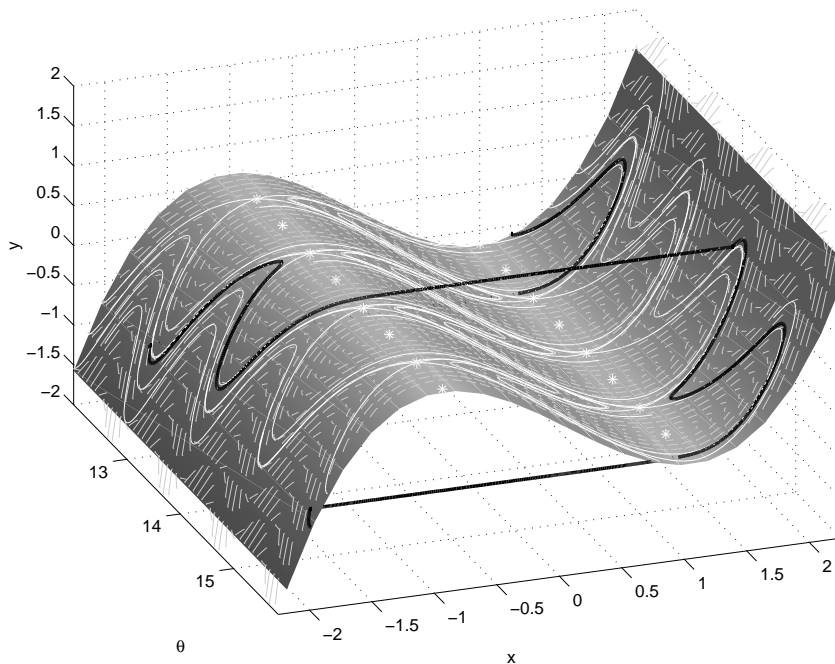
Figure 1.1. Three dimensional plot of a trajectory for the van der Pol equation and the critical manifold of the system. The folded saddles occur near the points on the critical manifold where the trajectory turns.

DAE does not adequately resolve the canards: they all appear to occur on trajectories of the slow flow that are asymptotic to the folded singularities. Singular perturbation analysis [5] determines asymptotic properties of the canards for small values of $\varepsilon > 0$ in the van der Pol equation. We shall not discuss these asymptotics or the geometry of canards in this paper, but note they are essential parts of the chaotic dynamics found in the van der Pol equation. It is relatively easy to compute the limiting images of the canards for the DAE, but we do not pursue this matter here.

The Jacobian of the slow flow equations is

$$\begin{pmatrix} 0 & 2\omega x \\ 2\pi a \cos(2\pi\theta) & -1 \end{pmatrix}.$$

The trace of the Jacobian is negative, so the slow flow is area contracting. This has two immediate implications about the phase portraits of the slow flow.

- There are no equilibrium points that are sources.

- There are no unstable periodic orbits. For $a < 1$, the flow points into the strip $x < \pm 1$ on its boundary, so the Poincaré-Bendixson Theorem implies that there is a stable periodic orbit in the strip.

As a increases, we encounter the following local degeneracies in the slow flow at points of the fold curves $S_{\pm 1}$ and the projections $S_{\mp 2}$ of the fold curves to stable sheets of the critical manifold [14, 16]:

- At $a = 1$, there is a folded saddle-node, dividing slow flows with no folded singularities from slow flows with two folded singularities, one a folded saddle $p_s = (\theta_s, 1) = (\frac{1}{2\pi} \sin^{-1}(\frac{1}{a}), 1)$ and the other a folded node or focus at $p_a = (\theta_a, 1) = (\frac{1}{2} - \frac{1}{2\pi} \sin^{-1}(\frac{1}{a}), 1)$.
- At $a = \sqrt{1 + 1/(16\pi\omega)^2}$, there is a resonant folded node dividing slow flows with folded nodes from slow flows with folded foci.
- At $a = 2$, the projections of the folds at $S_{\pm 1}$ of the slow flow onto the sheets of the critical manifold at $S_{\mp 2}$ have inflection points. At values of $a > 2$, the mappings along the slow flow from $S_{\pm 2}$ to $S_{\pm 1}$ are no longer monotone.

The separatrices of the folded saddle p_s play a significant role in the dynamics of the DAE and the van der Pol equation. In the half plane $1 \le x$, there is a stable separatrix W_s that arrives at p_s from the left and an unstable separatrix W_u that leaves p_s to the right. Figure 1.2 shows the saddle separatrices of (1.2) for parameter values $(\omega, a) = (1, 1.25)$ and $(\omega, a) = (2, 10)$. We note that W_u always intersects the circle S_1 before making a full turn around the cylinder $S^1 \times \mathbb{R}$. [1]

1.3   Symmetry and Return Maps

All trajectories with initial conditions on $S_{\pm 2}$ reach $S_{\pm 1}$ except those that lie in the stable manifold of a folded saddle or the strong stable manifold of a folded node. Let P_+ be the map along trajectories of the slow flow from S_2 to S_1, P_- the map along trajectories of the slow flow from S_{-2} to S_{-1}, $J_+(\theta, 1) = (\theta, -2)$ and $J_-(\theta, -1) = (\theta, 2)$. The return map for the DAE to the circle S_2 is then given by the composition $J_-P_-J_+P_+$. The slow flow and the DAE are symmetric with respect to the transformation $T(\theta, x) = (\theta + \frac{1}{2}, -x)$. Moreover, T^2 is the identity on $S^1 \times \mathbb{R}$, $TP_+ = P_-T$ and $TJ_+ = J_-T$. This implies that the return map $J_-P_-J_+P_+ = J_-P_-TTJ_+P_+ = (TJ_+P_+)(TJ_+P_+)$ is the square of the map $H = (TJ_+P_+)$ on the circle

---

[1] Here is the proof. Assume that W_u intersects the line $\theta = \frac{1}{2}$ and denote the segment of W_u that extends from p_s to $\theta = \frac{1}{2}$ by W_{u2}. Set $\bar{W}_{u2}$ to be the reflection of W_{u2} in the line $\theta = \frac{1}{2}$. If (θ, x) and $(1 - \theta, x)$ are symmetric points on W_{u2} and $\bar{W}_{u2}$, the vector $(\omega(x^2 - 1), x - a\sin(2\pi\theta))$ is tangent to $\bar{W}_{u2}$. But the vector field of the slow flow at this point is $(\omega(x^2 - 1), -x - a\sin(2\pi\theta))$, which points below the curve $\bar{W}_{u2}$. We conclude that W_u intersects the circle S_1 at a point $p_{1u} \in (\theta_s, 1 - \theta_s)$, proving our assertion.
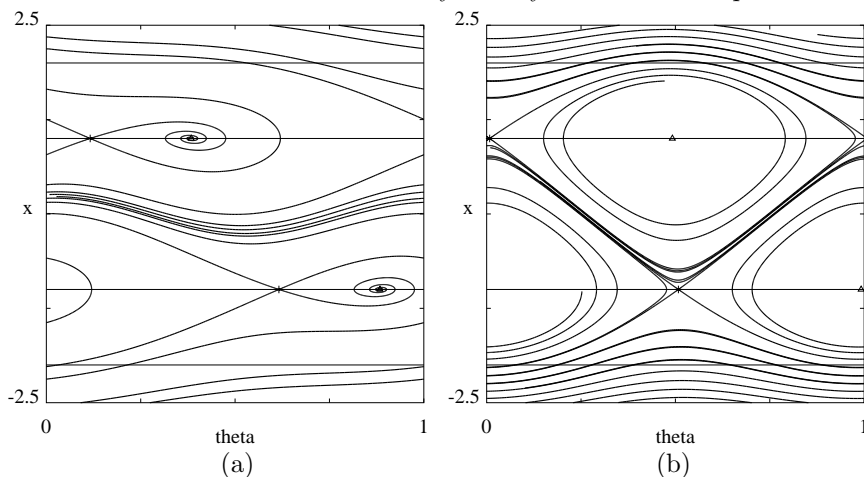
Figure 1.2. Phase portraits of the slow flow for parameter values (a) $(\omega, a) = (1, 1.5)$ and (b) $(\omega, a) = (5, 20)$. The stable and unstable manifolds of the folded saddles and the circles $|x| = 1$, $|x| = 2$ are drawn.

S_2. Consequently, the periodic orbits of the DAE can be divided into those that are fixed by the half return map H and those that are not. Because T phase shifts θ by $\frac{1}{2}$, the fixed points of H all yield periodic orbits whose period is an odd multiple of the forcing period $1/\omega$. The stable periodic orbits studied in the work of Cartwright and Littlewood [2, 10, 11] are the ones containing points fixed by H. In this paper, we shall also focus upon these orbits. Figure 1.4 shows graphs of the maps H for several parameter values.

There are three primary parameter ranges for a in which the maps P_+ and H have different properties. The map P_+ is a diffeomorphism of the circle S_2 to the circle S_1 for $0 < a < 1$. In this regime, x decreases along all trajectories in the strip $1 < x < 2$, implying that H is a circle diffeomorphism. Its rotation number depends upon ω, increasing with ω. All rotation numbers in $[\frac{1}{2}, \infty)$ are realized as ω varies in $(0, \infty)$.

When $1 < a < 2$, the map P_+ no longer maps the circle S_2 onto the circle S_1. Its image I_1 excludes the portion of S_1 that lies below the manifold W_u defined in the previous section. The discontinuities in the domain of P_+ occur at points in $W_s \cap S_2$. There is a single point of discontinuity since the circle S_2 is a cross-section for the flow. It also follows that the map P_+ remains increasing in this parameter regime. Thus, H is a family of increasing maps of the circle into itself with a single point of jump discontinuity in this parameter regime. This implies that H still has a well defined rotation number and periodic orbits of at most one period. Quasiperiodic trajectories are still possible, but the set of parameter values

yielding quasiperiodic trajectories is likely to have measure zero [7].

When $2 < a$, the map P_+ is no longer monotone. There are two points $p_{2l} = (\frac{1}{2\pi}\sin^{-1}(\frac{2}{a}), 2)$ and $p_{2r} = (\frac{1}{2} - \frac{1}{2\pi}\sin^{-1}(\frac{2}{a}), 2)$ at which P_+ has a local maximum and minimum, respectively. On the interval $D = (\theta_{2l}, \theta_{2r})$, P_+ has negative slope while on $S^1 - D$, it has positive slope. There are two crucial additional aspects to the structure of H as a piecewise continuous and piecewise monotone mapping of the circle. First, there are discontinuities of P_+ at intersections of D with W_s. (There may be only one such intersection point.) At the points of discontinuity in $W_s \cap S_2$, there is a jump with limit values $\frac{1}{2} + \theta_s = \theta_r$ and $\frac{1}{2} + p_{1u} = \theta_l$. We denote by q_l and q_r the points $(\theta_l, 2)$ and $(\theta_r, 2)$ in S_2. Second, we observe that the maximum height of W_u is a decreasing function of ω and is unbounded as $\omega \to 0$. Therefore, if $\omega > 0$ is small enough, W_u intersects the circle S_2. When this happens, it divides S_2 into two intervals. The points in S_2 above W_u have image in $I_H = [q_l, q_r]$ while the points in S_2 below W_u have image to the left of q_l. (If $0 < \theta_s < \frac{1}{2} < \theta_{1u} < 1$, then this expression yields $I_H \subset [0, 1]$. Otherwise, if $0 < \theta_{1u} < \frac{1}{2}$, the circular arc I_H contains 0 and it is convenient to choose a fundamental domain for the universal cover of the circle S_2 that contains $[q_l, q_r]$.) Note that W_s lies above W_u.

Figure 1.3a shows the structure of the flow in strip $1 < x < 2$ for $(\omega, a) = (5, 20)$, while figure 1.3a shows the structure of the flow in strip $1 < x < 2$ for $(\omega, a) = (10, 20)$. In this figure, the folded saddles p_s are located by the symbol $\times$. Their stable separatrices are drawn as solid curves, and their unstable manifolds are drawn as dot-dashed curves. The circles S_2 are drawn dotted, and the points p_{2l} and p_{2r} are labeled. The dashed trajectories have initial condition p_{2l}. The intervals $I_H = [q_l, q_r]$ that are the images of H are drawn as thick lines. The points $p_{1u} \in W_u \cap S_1$ are labeled and the points in $W_s \cap S_2$ are marked by large dots. The graph of the half-return map H for $(\omega, a) = (5, 20)$ is shown in Figure 1.4a. The map H is discontinuous at the points of $W_s \cap S_2$, has a local maximum at p_{2l} and a local minimum at p_{2r}.

We conclude that the graph of H can contain the following types of intervals on which it is monotone and continuous:

- a decreasing branch with domain $[p_{2l}, p_{2r}]$ (this occurs if W_s intersects S_2 in a single point),
- a branch containing p_{2r} with a local minimum,
- a branch containing p_{2l} with a local maximum,
- monotone decreasing branches in $[p_{2l}, p_{2r}]$,
- monotone increasing branches in the complement of $[p_{2l}, p_{2r}]$.

We assume for the moment that all intersections of Ws with S2 are transverse. Then W_s must have an odd number of interections with S2 and every intersection in $[\theta_{2l}, \theta_{2r}]$ is preceded by an intersection in the complement of this interval. Therefore, the number of monotone increasing branches is
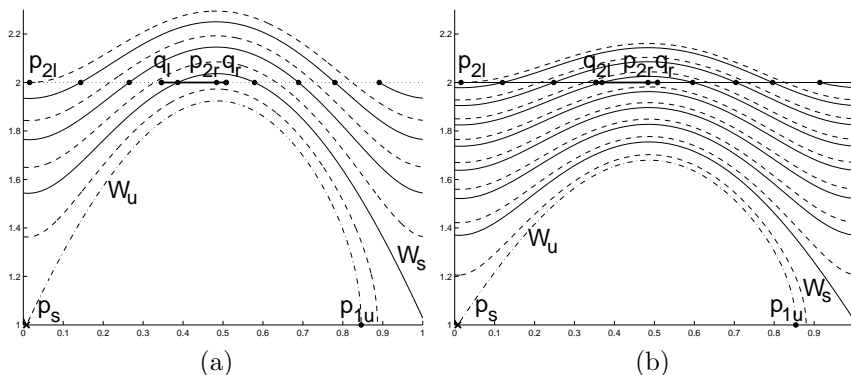
Figure 1.3. The structure of the slow flow in the strip $1 < x < 2$ for (a)$(\omega, a) = (5, 20)$ and (b)$(\omega, a) = (10, 20)$. Unstable manifolds W_u are drawn with dot-dash curves, stable manifolds W_s are drawn solid, the trajectories originating at the points p_{2l} are drawn dashed and the circles $x = 2$ are drawn as dotted lines.

one larger than the number of monotone decreasing branches. Moreover, the image of all branches is contained in I_H except the branch with a local minimum.

We next analyze the properties of the map H near a point $p \in W_s \cap S_2$. If $p \in [p_{2l}, p_{2r}]$, then the limit value on the left is q_l and the limit value on the right is q_r. If $p \in [p_{2r}, p_{2l}]$, then the limit value on the right is q_l and the limit value on the left is q_r. The slope of the map H on the two sides of p behaves very differently. The points with limit value q_r cross S_1 just to the left of p_s. Since the line S_1 is transverse to the stable and unstable manifolds of p_s, the flow map P_+ has a singularity of the form $(\theta_s - \theta)^\alpha$ with $0 < \alpha < 1$. [2] The points with limit value q_l follow the unstable manifold W_u of p_s to its first crossing with S_1. The map along the flow also has a power law singularity. The exponent is the ratio of the magnitudes of the stable and unstable eigenvalues of p_s. Since the trace of the Jacobian is negative, the stable eigenvalue has larger magnitude and the exponent is larger than 1. We conclude that the map H has unbounded slope as $H(\theta)$ approaches q_r, and slope approaching zero as $H(\theta)$ approaches q_l.

---

[2] This is readily computed if we assume that the flow is linear near p_s. Let (u, v) be coordinates with the stable manifold the u-axis and the unstable manifold the v-axis. Assume that the eigenvalues are $\mu > 0$ and $\lambda < 0$. The trajectories of the flow are then graphs of functions $v = cu^{\mu/\lambda}$. The flow from the cross-section $u = 1$ to the line $v = mu$ sends the point $(1, c)$ to $((c/m)^{-\lambda/(\mu-\lambda)}, m(c/m)^{-\lambda/(\mu-\lambda)})$. Since $\lambda < 0 < \mu$, $0 < -\lambda/(\mu - \lambda) < 1$.

1.4   Degenerate Decompositions and Fixed Points of H

This section considers the fixed points of the half-return map H, which correspond to periodic orbits of odd period for the DAE of the forced van der Pol equation. The previous section describes the structure of H as a piecewise continuous, piecewise monotone mapping. There is a substantial difference between cases for $a < 1$, $1 < a < 2$ and $2 < a$. For $a < 1$, H is a diffeomorphism and for $2 > a > 1$, H has a single point of discontinuity. There will be ranges of values of ω in these cases for which H has a fixed point, one interval for each odd multiple of the forcing period. The case $a > 2$ is the one of most interest to us, and we assume $a > 2$ in the remainder of this section.

There are two types of bifurcations that affect the number of fixed points of H:

- Bifurcations in the interior of intervals of monotonicity are saddle-nodes where the slope of H is 1 or period-doubling bifurcations where the slope of H is -1.
- Bifurcations that involve endpoints of the intervals of monotonicity correspond to homoclinic bifurcations of the DAE.

We have not encountered period doubling bifurcations, but have found saddle-nodes. We have found homoclinic bifurcations where the periodic orbits approach p_s from the left and also ones where the periodic orbits approach p_s from the right.

In addition to bifurcations, there are parameter values at which the number of discontinuities and turning points of H change. These correspond to *degenerate decompositions* for the DAE. For example, when $a = 1$, the DAE has a saddle-node and its preimage under P_+ is a singular point of H. Despite the fact that a saddle-node has a half-space of trajectories that approach the saddle-node point, all of the trajectories starting at S_2 reach S_1 under the slow flow except for the one on the strong stable manifold of the equilibrium point. The other degenerate decompositions we consider involve tangencies of the slow flow with the circle S_2.

The general structure of H for $a > 2$ was described in the previous section. There is one local maximum, one local minimum and an odd number of jump discontinuities with the same limit values at each discontinuity. Here we examine how the number of intervals of monotonicity and the number of fixed points of H change. The discontinuities occur at points in $W_s \cap S_2$. As the parameters vary, the number of these points changes only when there is a point where W_s is tangent to S_2. The tangency points of the slow flow with S_2 are p_{2l} and p_{2r}. When ω increases with a fixed, the stable manifold W_s tends to move downwards. Consequently, points of $W_s \cap S_2$ appear at p_{2l} where trajectories of the vector field are tangent to S_2 from above and disappear at p_{2r} where where trajectories of the vector

field are tangent to S_2 from below. Before a new branch appears at θ_{2l}, $H(\theta_{2l})$ approaches q_l. The new branch appears with $H(\theta_{2l})$ taking a value near $\theta_l = \theta_{1u} - \frac{1}{2}$. New branches can disappear at θ_{2r} only in the regime where W_u does not intersect S_2 since W_s lies above W_u and p_{2r} lies below W_u when $W_u \cap S_2$ is nonempty. As ω increases, the domain of the branch with local minimum at θ_{2r} shrinks and $H(\theta_{2r})$ approaches θ_r. When the branch disappears, $H(\theta_{2r})$ jumps down to θ_l.

In addition to changes in the number of branches of H associated with tangencies of W_s with S_2, there also are parameter values at which the point p_{2r} is in the forward trajectory of p_{2l} and parameter values at which W_u is tangent to S_2. Combinations of these degeneracies are also possible at isolated points. For example, near $(\omega, a) = (3, 15)$ there appear to be parameter values for which W_s passes through p_{2l} and W_u passes through p_{2r}.

We observe in our numerical computations that the point $p_{1u} = W_u \cap S_1$ does not change much with varying ω. The points of intersection in $W_s \cap S_2$ vary much more quickly. Thus, in describing the bifurcations of fixed points of H, we shall speak as if p_{1u} is independent of ω though this is not the case. The only fixed points of H that we have observed occur in the branch containing p_{2r} and the branch immediately to the left of this one. We denote the domains of these two branches by I_m and I_{lm}, respectively. The branch of H with domain I_m is a unimodal map with a turning point at p_{2r} with $\theta_{2r} < \frac{1}{2}$. As ω increases, I_m shrinks. The value of H at the endpoints of I_m is $\theta_r = \theta_s + \frac{1}{2} > \frac{1}{2}$. As the branch shrinks, its minimum value also approaches q_r. Therefore, the branch contains no fixed points when it is short enough. On the other hand, for many parameter values the branch is wide enough that its right endpoint is to the right of the diagonal. The graph of $H|I_m$ must then cross the diagonal an odd number of times, so we expect a single fixed point. There are two bifurcations that occur as the branch shrinks: at the first bifurcation, the right endpoint of the graph of $H|I_m$ meets the diagonal, and a second fixed point appears at the right end of the branch. This fixed point is unstable since the slope of H is unbounded near the endpoints of I_m. The second bifurcation is a saddle-node that occurs as the two fixed points collide and the graph of $H|I_m$ moves completely above the diagonal.

As I_m shrinks with increasing ω, the right endpoint of I_{lm} moves to the right. It crosses the diagonal, creating a fixed point of H in I_{lm}. This often occurs before the homoclinic and saddle-node bifurcation within I_m. Since H is decreasing on I_{lm}, it can contain only this single fixed point of H. Because the slope of H approaches 0 at the right endpoint of I_{lm}, the fixed point in I_{lm} is stable when it is created. Thus, our observations indicate that as ω varies, there are parameter regions in which H has two stable fixed points, and in part of this region, there is also an unstable fixed point in I_m. Figure 1.4 displays graphs of H for four different values of (ω, a):

$a = 20$ and $\omega = 5, 5.38, 5.4, 5.5$. At $\omega = 5$, there is bistability and the right end of the branch I_m lies below the diagonal. At $\omega = 5.38$, I_m has shrunk, and its right endpoint is almost on the diagonal. At $\omega = 5.4$, the branch I_m has shrunk still further and lies just above the diagonal. At $\omega = 5.5$, the number of branches has changed as the former I_m disappeared.
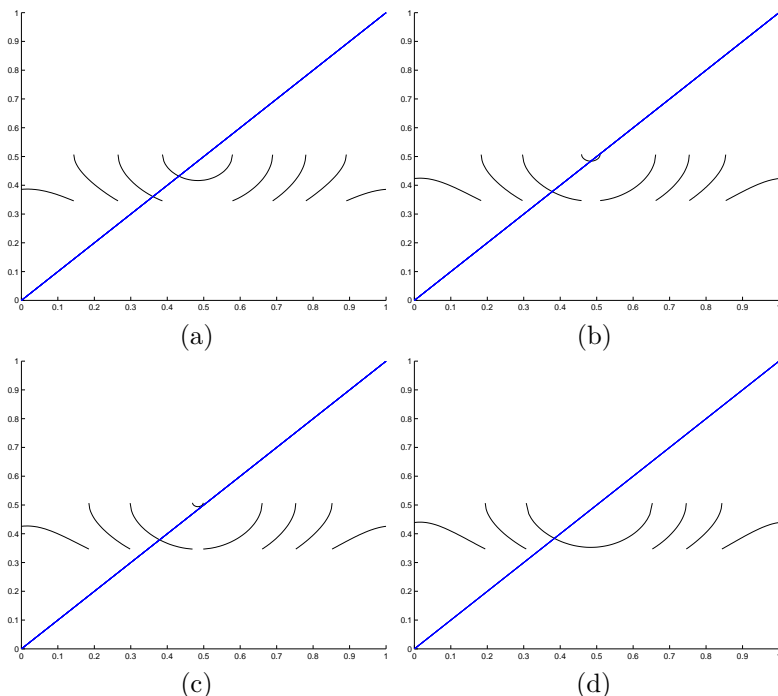
Figure 1.4. Graphs of the half-return map for parameter values $a = 20$ and (a) $\omega = 5$, (a) $\omega = 5.38$, (a) $\omega = 5.4$, (a) $\omega = 5.5$.

The periods of the branches are evident in Figure 1.3. In Figure 1.3a, the value of θ changes by less than 1 as points in I_m flow from S_2 to S_1. The value of θ changes by an amount between 1 and 2 as points in I_{lm} flow from S_2 to S_1. Therefore, the fixed point in I_m has θ-period 1 and the fixed point in I_{lm} has θ-period 3. These two periodic orbits are displayed in Figure 1.5. In Figure 1.3b, the theta periods in I_m and I_{lm} are 9 and 11, respectively.

We end this section with an observation about the limit of the slow flow equations in which $a \to \infty$ and $\omega \to \infty$ with the ratio ω/a constant. If we rescale the equations by dividing by a and denote $\delta = 1/a$, the slow
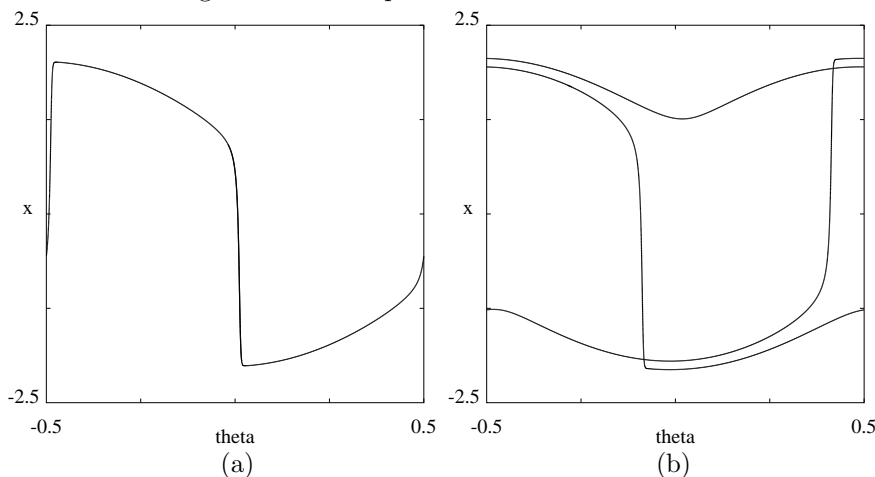
Figure 1.5. Stable periodic orbits of (a) ω-period 1 and (b) ω-period 3 for parameter values $(\omega, a) = (5, 20)$.

flow equations become

$$
\begin{aligned}
\theta' &= \beta(x^2 - 1) \\
x' &= -\delta x + \sin(2\pi\theta),
\end{aligned}
\tag{1.3}
$$

where $\beta = \omega/a$. The limit $\delta = 0$ is a Hamiltonian system, with Hamiltonian

$$
E(\theta, x) = \frac{\cos(2\pi\theta) - 1}{2\pi} + \beta \left(x^3/3 - x + 2/3 \right),
$$

so we can use perturbation analysis to characterize the phase portraits of the system when δ is small. We have only begun to carry out this analysis and record here some of the properties of the case $\delta = 0$:

- There is a saddle at $(\theta, x) = (0, 1)$ with a homoclinic connection γ_u above the center at $(0.5, 1)$. The constant part of $E(\theta, x)$ was chosen so that $E(\theta, x) = 0$ on the saddle and the homoclinic connection.
- When $\beta > 3/(4\pi)$, there is also a homoclinic connection γ_l that encircles the cylinder and goes below $(0.5, 1)$. The homoclinic connection γ_u does not intersect the line $x = 2$. See Figure 1.6(a).
- When $\beta = 3/(4\pi)$, the homoclinic connection γ_u is tangent to $x = 2$ at $\theta = 0.5$. Moreover, the lower homoclinic connection γ_l meets the saddle at $(0.5, -1)$, forming a heteroclinic cycle. See Figure 1.6(b).
- When $0 < \beta < 3/(4\pi)$, the homoclinic orbit γ_u intersects $x = 2$ twice. Moreover, the saddle at $(0.5, -1)$ has a homoclinic connection γ_0 that encircles the center $(0.5, 1)$ and is tangent to $x = 2$ at $\theta = 0.5$. This homoclinic connection does not encircle the cylinder. It intersects

the fold line $x = 1$ at the points where $\cos(2\pi\theta) = 8\pi\beta/3 - 1$. See Figures 1.6(c) and 1.6(d).
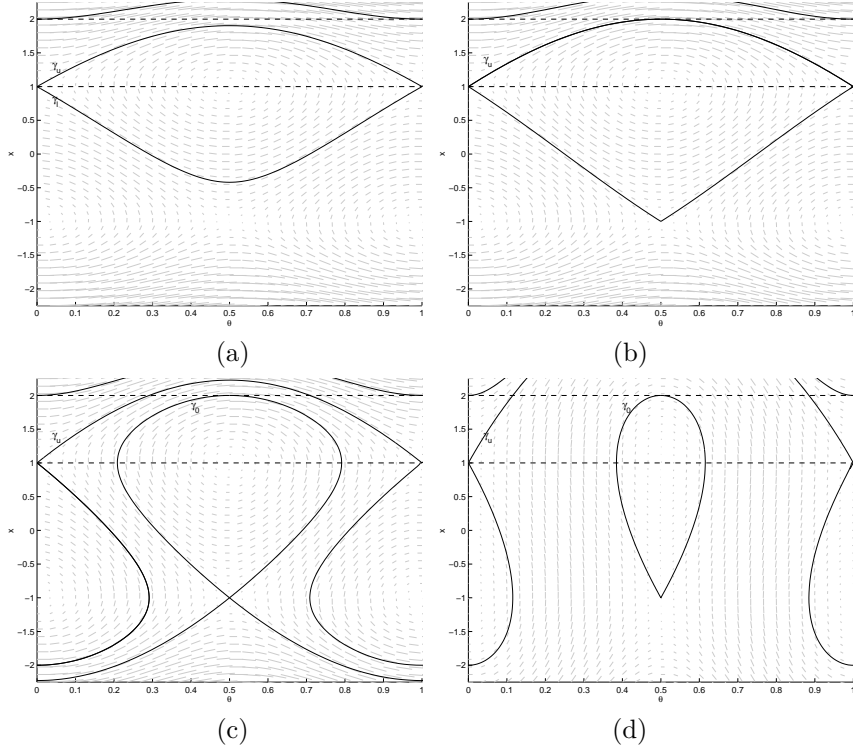
Figure 1.6. Phase portraits of the system (1.3) with $\delta = 0$: (a) $\beta = 0.30 > 3/(4\pi)$;   (b) $\beta = 3/(4\pi)$;   (c) $\beta = 0.15 < 3/(4\pi)$;   (d) $\beta = 0.03 \ll 3/(4\pi)$.

1.5   Concluding Remarks

This paper is an initial step towards determining the global bifurcation diagram for the forced van der Pol equation near its singular perturbation limit. We exhibit stable periodic orbits in the singular limit of the differential algebraic equation and establish that their existence is due primarily to a phenomenon that has received little attention in the literature on singularly perturbed dynamical systems. In particular, the "projection" of a fold curve along the fast flow of the system is tangent to the slow flow on a sheet of the critical manifold. These tangencies lead to a lack of monotonicity in the return map for the system along folds of the critical manifold. Our

work appears to be the first time that such tangencies have been noted in the van der Pol equation and related to its bifurcations. By viewing the system in terms of return maps to the fold curves rather than by fixing a cross-section of constant phase, the tangencies become evident.

We conjecture that the parameter region with stable periodic orbits that have θ-period $2n + 1$ forms a strip in the (ω, a) plane that extends from the ω-axis to ∞ with increasing a. One boundary of these strips is conjectured to be a saddle-node bifurcation of periodic orbits and the other boundary is a bifurcation that approaches a homoclinic orbit of the differential algebraic equation as $\varepsilon \to 0$. We have not yet characterized these bifurcations outside the singular limit, but conjecture that they become saddle-nodes as the stable periodic orbits collide with unstable periodic orbits at the edge of regions where there are periodic orbits with canards. For each pair of adjacent odd integers $2n \pm 1$, we further conjecture that there is a number $a_n > 2$ such that the strips overlap for $a > a_n$ and that no overlaps occur for $a < a_n$. For the differential algebraic equation, there is a codimension two point with $a = a_n$ at which the period $2n - 1$ orbit has a saddle-node and the period $2n + 1$ orbit has a homoclinic bifurcation.

The differential algebraic equation can be used to give approximations to the locations of canards in the van der Pol equation. The stable separatrix of the folded saddle in the strip $|x| < 1$ gives the approximate location of the canards, and the jumps from the canards to the stable sheets of the critical manifold can be calculated explicitly within the differential algebraic equation. This information is a starting point for asymptotic analysis that should lead to global bifurcation diagrams of the van der Pol equation in the relaxation oscillation regime with $\varepsilon > 0$ small. Additional perturbation analysis should characterize the properties of the system in the parameter regions where ω and a are large, but have a bounded ratio.

[1] Arnold V Afrajmovich V Ilyashenko Yu Shil'nikov L 1994 *Bifurcation Theory: Dynamical Systems V* (Springer-Verlag, Encyclopaedia of Mathematical Sciences)

[2] Cartwright M and Littlewood J 1945 On nonlinear differential equations of the second order: I the equation $\ddot{y} - k(1 - y^2)\dot{y} + y = bk\cos(\lambda t + a)$, k large. *J. London Math. Soc.* **20** 180–9

[3] Cartwright M and Littlewood J 1947 On nonlinear differential equations of the second order: II the equation $\ddot{y} - kf(y, \dot{y})\dot{y} + g(y, k) = p(t) = p_1(t) + kp_2(t)$, $k > 0, f(y) \geq 1$. *Ann. Math.* **48** 472–94 [Addendum 1949 **50** 504–5

[4] Flaherty J and Hoppensteadt F 1978 Frequency entrainment of a forced van der Pol oscillator *Stud. Appl. Math.* **58** 5–15

[5] Grasman J 1987 *Asymptotic Methods for Relaxation Oscillations and Applications* (Springer-Verlag)

[6] Guckenheimer J Hoffman K Weckesser W 2000 Numerical computation of canards, *Int. J. Bif. Chaos*, to appear.

[7] Keener J 1980 Chaotic behavior in a piecewise continuous difference equation *Trans. Amer. Math. Soc.* **261** 589–604

[8] Levi M 1981 Qualitative analysis of the periodically forced relaxation oscillations *Mem. Amer. Math. Soc.* **214** 1–147

[9] Levinson N 1949 A second order differential equation with singular solutions *Ann. Math.* **50** 127–153

[10] Littlewood J 1957 On nonlinear differential equations of the second order: III the equation $\ddot{y} - k(1 - y^2)\dot{y} + y = bk\cos(\lambda t + a)$ for large k and its generalizations. *Acta math.* **97** 267–308 [Errata at end of 1957, 2.]

[11] Littlewood J 1957 On nonlinear differential equations of the second order: III the equation $\ddot{y} - kf(y)\dot{y} + g(y) = bkp(\phi), \phi = t + a$ for large k and its generalizations. *Acta math.* **98** 1–110

[12] Mettin R Parlitz U Lauterborn W 1993 Bifurcation structure of the driven van der Pol oscillator *Int. J. Bif. Chaos* **3** 1529–1555

[13] Mischenko E Rozov N 1980 *Differential Equations with Small Parameters and Relaxation Oscillations.* (Plenum Press)

[14] Mischenko E Kolesov Yu Kolesov A Rozov N 1994 *Asymptotic methods in singularly perturbed systems* (Translated from the Russian by Irene Aleksanova. New York: Consultants Bureau)

[15] Smale S 1963 Diffeomorphism with many periodic points In *Differential and Combinatorial Topology* S Cairns (ed.) (Princeton: Princeton University Press) 63–80

[16] Szmolyan P Wechselberger M 2000 Canards in R^3 *preprint*

[17] Takens F 1974 Forced oscillations and bifurcations *Comm. Math. Inst. Rijkuniversiteit Utrecht* **3** 1–59

[18] Takens F 1975 *Constrained equations; a study of implicit differential equations and their discontinuous solutions* Report ZW-75-03 (Groningen: Mathematisch Institut, Rijksuniversiteit)

[19] van der Pol B van der Mark J 1927 Frequency demultiplication *Nature* **120** 363–364